Accepted for publication in Angewandte Chemie

Formic Acid Dehydrogenation on Au-Based Catalysts at Near-Ambient Temperatures

Manuel Ojeda and Enrique Iglesia*

Department of Chemical Engineering, University of California

and

Chemical Sciences Division, E.O. Lawrence Berkeley National Laboratory,

Berkeley, CA, USA

* corresponding author (iglesia@berkeley.edu)

Formic acid (HCOOH) is a convenient hydrogen carrier in fuel cells designed for portable use. [1-4] Recent studies have shown that HCOOH decomposition is catalyzed with Ru-based complexes in the aqueous phase at near-ambient temperatures. [5,6] HCOOH decomposition reactions are used frequently to probe the effects of alloying and cluster size and of geometric and electronic factors in catalysis [7-10]. These studies have concluded that Pt is the most active metal for HCOOH decomposition, at least as large crystallites and extended surfaces [9]. The identity and oxidation state of surface metal atoms influence the relative rates of dehydrogenation ($HCOOH \rightarrow H_2 + CO_2$) and dehydration ($HCOOH \rightarrow H_2O + CO$) routes, a selectivity requirement for the synthesis of CO-free H_2 streams for low-temperature fuel cells. Group Ib and Group VIII noble metals catalyze dehydrogenation selectively, while base metals and metal oxides catalyze both routes, either directly or indirectly via subsequent water-gas shift (WGS) reactions [8,11-13].

Mars *et al.* [8] concluded that formates act as intermediates in HCOOH decomposition; their formation limits rates on nobler metals (Au, Ag) and its decomposition on the others. Au catalysts previously gave lower areal rates than other metals, as expected from its inertness for HCOOH dissociation, evident in its first-order HCOOH decomposition kinetics [14]. Small Au clusters (<5 nm) deposited on oxide supports catalyze many reactions at turnover rates higher than larger clusters, apparently because coordinatively unsaturated or non-zero valent species bind molecules more strongly than low-index surfaces on larger crystallites [15-18].

This study shows that well-dispersed Au species grafted onto γ-Al_2O_3 give significantly higher HCOOH metal-time yields (on the basis of the total number of metal atoms) [19] than even Pt clusters. Decomposition occurs at near ambient temperatures (~350 K) and forms only H_2 and CO_2, suitable for direct use in fuel cells. In contrast with pathways on Pt, HCOOH decomposes on dispersed Au species via H-assisted bimolecular formate decomposition instead of via well-

established unimolecular analogs. This remarkable reactivity arises from dispersed Au species, undetectable by electron microscopy, which grew during thermal treatments, instead of from the predominant Au metal clusters (3-4 nm) evident in micrographs, which are unaffected by thermal treatments and catalyze CO oxidation.

HCOOH decomposition metal-time yields on well-dispersed Au species (Figure 1) are much higher than on Pt clusters at all temperatures (343-383 K). These higher metal-time yields do not reflect metal dispersion differences (0.28 for Au and 0.21 for Pt, based on size of clusters visible in transmission electron micrographs (TEM)). Activation energies in the zero-order HCOOH kinetic regime were 53±2 and 72±4 kJ mol^{-1} for Au and Pt, respectively, in reasonable agreement with previous reports (40-60 and 58-73 kJ mol^{-1} for Au and Pt, respectively [14,20-22]).

HCOOH dehydrogenation turnover rates increased with decreasing Pt cluster size (Figure 2). Thermal treatment of Au/Al_2O_3 in flowing O_2/He flow at temperatures up to 1073 K led to a marked decrease in turnover rates without a concurrent increase in the size of Au clusters detectable by TEM (Supporting Information). This indicates that Au species active in HCOOH decomposition do not reside on surfaces of the TEM-visible clusters. HCOOH dehydrogenation and water-gas shift (WGS) reactions have been proposed to involve formate-type species. Indeed, we find that WGS rates also decreased markedly upon thermal treatment, while CO oxidation rates remain essentially unchanged (Figure 3). Thus, we conclude that CO oxidation, but not WGS or HCOOH dehydrogenation, occurs on active sites provided by the Au metal clusters detected in the micrographs. Our data indicate that HCOOH dehydrogenation and WGS reactions occur on similar Au species, undetectable by TEM and present as much smaller clusters or even atomically-dispersed structures, as proposed recently for WGS reactions on Au/CeO_2 catalysts [23]. These species account for the remarkable reactivity of Au-based catalysts

in HCOOH dehydrogenation. Such isolated Au species coalesce at higher temperatures to form Au metal clusters with much lower HCOOH dehydrogenation reactivity.

Au/TiO_2 catalysts (World Gold Council, treated in O_2/He at 523 K) with a cluster size distribution similar to that in Au/Al_2O_3 (treated in O_2/He at 873 K) gave lower metal-time yields for HCOOH dehydrogenation (7 *vs.* 201 mol g-at Au^{-1} h^{-1}), apparently because of smaller concentrations of isolated Au species than even on Au/Al_2O_3 samples treated at 873 K. In contrast, CO oxidation rates were similar on these two samples (~ 2.6 mol g-at Au_s^{-1} s^{-1} at 288 K, CO (5 kPa), O_2 (2 kPa) and H_2O (0.5 kPa)), consistent with active sites located in the Au clusters detected by TEM, which were of similar size in Au/TiO_2 and Au/Al_2O_3 samples (3-4 nm).

Au/Al_2O_3 and Pt/Al_2O_3 formed only H_2 and CO_2 from HCOOH and neither dehydration nor reverse WGS products were detected. Dehydrogenation rates were independent of HCOOH pressure (0.25-8 kPa) on Au/Al_2O_3 (Figure 4). In contrast, rates first increased with HCOOH pressure and then reached constant values at >2 kPa HCOOH on Pt/Al_2O_3. Zero-order HCOOH kinetics indicate that surfaces are saturated with reactive intermediates with rates determined by their decomposition, as in the case of (*a*) dissociative adsorption of HCOOH and decomposition of the resulting formates unimolecularly or bimolecularly on saturated surfaces, or (*b*) bimolecular reactions of saturated formates with HCOOH molecules adsorbed on a separate site also at saturated coverages.

H/D kinetic isotope effects (KIE) were used to discriminate among these mechanistic possibilities. Kinetically-relevant dissociation would give normal KIE values ($r_H/r_D>1$) for HCOOD, but not for DCOOH. Rate-limiting formate decomposition would lead to normal KIE values for DCOOH, but not for HCOOD. On Pt/Al_2O_3, small normal KIE values (Table 1), typical of thermodynamic isotope effects, were observed for HCOOD, and much larger values for both DCOOH and DCOOD, consistent with kinetically-relevant formate dehydrogenation via unimolecular C-H(D)

bond cleavage (mechanism *a*). On Au/Al_2O_3, all isotopomers gave KIE values of apparent kinetic origin. These KIE values on Au/Al_2O_3 do not reflect DCOOH ⇆ HCOOD scrambling during dehydrogenation, because isotopic mixing was not detected on either Au or Pt catalysts. Binomial dihydrogen isotopomers formed on Pt/Al_2O_3, while HD was the only dihydrogen isotopomer formed during HCOOD and DCOOH dehydrogenation on Au/Al_2O_3, indicating that surface H-atoms are unable to recombine on Au active sites. Dihydrogen must therefore form via reactions of methyl hydrogen atoms in formate groups with hydroxyl-derived H atoms, without isotopic mixing or recombinative desorption of H-atoms on Au active sites.

KIE values and dihydrogen isotopomers on Au/Al_2O_3 are inconsistent with sequential HCOOH dissociation and unimolecular formate decomposition. A sequence of elementary steps consistent with these kinetic and isotopic data on Au catalysts is shown in Scheme 1. HCOOH adsorbs dissociatively to give formates in quasi-equilibrated steps, which then decompose to give CO_2 and H_2 in a step assisted by H-atoms previously formed via HCOOH dissociation, and which do not recombine on Au to form dihydrogen. This kinetically-relevant step accounts for the normal KIE values measured for all formic acid isotopomers on Au catalysts and for the exclusive formation of HD from DCOOH and HCOOD. On Pt catalysts, quasi-equilibrated recombinative hydrogen desorption scrambles hydrogen isotopes and formate species are decomposed *via* unassisted pathways, because hydrogen recombination can complete catalytic cycles.

On Au catalysts, the assumption of pseudo-steady-state for all adsorbed species in Scheme 1 gives the following rate equation assuming HCOO* and H* as the most abundant surface intermediates:

$$r_{HCOOH} = \frac{K_1 k_2 P_{HCOOH}}{(1 + 2K_1^{1/2} P_{HCOOH}^{1/2})^2}$$

which simplifies to $r_{HCOOH} = k_2 / 4$ when rates become independent of HCOOH pressures, as suggested by the data in Figure 4. Thus, dehydrogenation rates depend on the rate constant for step 2 and on the isotopic identity of both hydroxyl and carbonyl hydrogens in formic acid.

The exclusive formation of HD from HCOOD and DCOOH indicates that dihydrogen forms in irreversible steps, a situation that gives rise to a chemical potential of hydrogen much higher at active sites (within the H-containing intermediates that form H_2) than in the H_2 present in the contacting gas phase, as shown by the non-equilibrium thermodynamic treatments of chemical kinetics of DeDonder and Boudart [24,25]. Thus, the driving force for any reaction using hydrogen as a reactant, whether at electrodes or in cross-hydrogenation reactions, would be much higher during HCOOH dehydrogenation than at the H_2 pressure prevalent during catalysis. We conclude that HCOOH can be used as an *in situ* source of hydrogen at high chemical potentials on isolated Au species, because these species do not equilibrate surface and gas phase hydrogen pools during HCOOH dehydrogenation.

In summary, well-dispersed Au species grafted onto γ-Al_2O_3, undetectable by electron microscopy, dehydrogenate HCOOH with much higher metal-time yields than Pt clusters, previously considered to be the most active catalyst for this reaction. HCOOH dehydrogenation proceeds via a H-assisted formate decomposition mechanism, leading to H_2/CO_2 streams well-suited for direct use in low-temperature fuel cells and to surface hydrogen chemical potentials of potential use in the upgrading of unsaturated or oxygenated molecules via cross-hydrogenation catalysis. These Au species also catalyze water-gas shift, but CO oxidation occurs instead on Au metal clusters detectable by transmission electron microscopy.

Experimental Section

The Au/Al_2O_3 catalyst (0.61 wt.%) was prepared by the deposition-precipitation (DP) [26]. $HAuCl_4 \cdot xH_2O$ (0.24 g, Aldrich, 99.999%) was dissolved in deionized H_2O (80 cm^3) at 353 K. The support (5 g, γ-Al_2O_3, Alcoa) was treated in air at 923 K for 5 h, and suspended in H_2O (120 cm^3) at 353 K. Au deposition onto Al_2O_3 was performed at 353 K and pH = 7 (adjusted with NaOH 0.5 M) by stirring both solutions together for 1 h. The solid was filtered and washed twice with water at room temperature and then once with warm water (323 K), followed by drying at room temperature for 24 h. The Au content is 0.61 wt.% (Galbraith Laboratories, Inc.). Three different portions were treated in O_2/He (25 vol.%, 25 cm^3 g^{-1} s^{-1}) by increasing the temperature from ambient to 873, 950 and 1023 K at 0.17 K s^{-1} and holding at each temperature for 2 h. The Au/TiO_2 material (1.56 wt.%, 3.3±0.7 nm) was prepared by DP and supplied by the World Gold Council. Pt catalysts (2 wt.%) with different metal cluster size were prepared by Nanostellar using colloidal methods [27].

HCOOH decomposition, WGS and CO oxidation rates were measured in a packed-bed reactor. The catalyst (30-100 mg) was diluted with quartz particles (washed with HNO_3 and treated in air at 1023 K for 5 h) and pretreated *in situ* in flowing pure H_2 at 373 K (heating rate of 0.17 K s^{-1}) for 0.5 h and then in a mixture H_2O/H_2 (1 vol.% H_2O) at 373 K for 0.5 h [28]. Gas reactants (He, 10 vol.% CO/He, 25 vol% O_2/He, Praxair, UHP) were introduced with mass-flow controllers, while liquid HCOOH (Acros, 99% pure) and H_2O were fed with a syringe pump (Cole Parmer 74900 Series). KIE were measured by using deuterated formic acid (Cambridge Isotope Laboratories, 98%). Reactants and products concentrations were determined *on line* with a mass spectrometer (Inficon Transpector) and a gas chromatograph (Hewlett-Packard 6890GC) equipped with a Porapak Q packed column (80–100 mesh, 1.82 m × 3.18 mm) connected to a thermal conductivity detector.

Acknowledgements

M. Ojeda acknowledges financial support from the European Union (Marie Curie Actions). This work was supported by the Director, Office of Basic Energy Sciences, Chemical Sciences Division of the U.S. Department of Energy under Contract DE-AC02-05CH11231. We acknowledge H. Kung and M. Kung (Northwestern University) for an initial catalyst sample and for detailed procedures that allowed us to reproduce their synthesis protocols. The expert assistance of M. Avalos, L. Rendon and F. Ruiz from the Centro de Ciencias de la Materia Condensada, UNAM, Mexico in transmission electron microscopy is also acknowledged with thanks.

References

[1] C. Rice, R.I. Ha, R.I. Masel, P. Waszczuk, A. Wieckowski, T. Barnard, *J. Power Sources* **2002**, *111*, 83.
[2] X. Yu, P.G. Pickup, *J. Power Sources* **2008**, *182*, 124.
[3] S. Enthaler, *ChemSusChem* **2008**, *1*, 801.
[4] F. Joó, *ChemSusChem* **2008**, *1*, 805.
[5] B. Loges, A. Boddien, H. Junge, M. Beller, *Angew. Chem. Int. Ed.* **2008**, *47*, 3962.
[6] C. Fellay, P.J. Dyson, G. Laurenczy, *Angew. Chem. Int. Ed.* **2008**, *47*, 3966.
[7] R.J. Madix, *Catal. Rev. Sci. Eng.* **1984**, *26*, 281.
[8] P. Mars, J.J.F. Scholten, P. Zwietering, *Adv. Catal.* **1963**, *14*, 35.
[9] M.A. Barteau, *Catal. Letters* **1991**, *8*, 175.
[10] E. Iglesia, M. Boudart, *J. Phys. Chem.* **1991**, *95*, 7011.
[11] J.M. Trillo, G. Munuera, J.M. Criado, *Catal. Rev.* **1972**, *7*, 51.
[12] R. Larsson, M.H. Jamroz, M.A. Borowiak, *J. Molec. Catal. A: Chem.* **1998**, *129*, 141.
[13] K.S. Kim, M.A. Barteau, *Langmuir* **1988**, *4*, 945.
[14] W.M.H. Sachtler, J. Fahrenfort, *Actes du Deuxieme Congres Internationale de Catalyse* **1961**, 831.
[15] H.H. Kung, M.C. Kung, C.K. Costello, *J. Catal.* **2003**, *216*, 425.
[16] G.C. Bond, D.T. Thompson, *Gold Bull.* **2000**, *33*, 41.
[17] D. Andreeva, *Gold Bull.* **2002**, *35*, 82.

[18] A.S.K. Hashmi, G.J. Hutchings, *Angew. Chem. Int. Ed.* **2006**, *45*, 7896.

[19] M. Boudart, G. Djéga-Mariadassou, *Kinetics of heterogeneous catalytic reactions*; Princeton University Press: Princeton, N.J., 1984.

[20] W.J. Chun, K. Tomishige, M. Hamakado, Y. Iwasawa, K. Asakura, *J. Chem. Soc., Faraday Trans.* **1995**, *91*, 4161.

[21] M.M. Mohamed, M. Ichikawa, *J. Colloid Interf. Sci.* **2000**, *232*, 381.

[22] J. Block, J. Vogl, *Z. Elektrochem.* **1959**, *63*, 3.

[23] Q. Fu, H. Saltsburg, M. Flytzani-Stephanopoulos, *Science* **2003**, *301*, 935.

[24] M. Boudart, *Catal. Letters* **1989**, *3*, 111.

[25] S.Y. Yu, J.A. Biscardi, E. Iglesia, *J. Phys. Chem. B* **2002**, *106*, 9642.

[26] M. Haruta, *Catal. Today* **1997**, *36*, 153.

[27] A.D. Allian, K. Takanabe, K.L. Fujdala, X. Hao, T.J. Truex, E. Iglesia, *in preparation* **2008**.

[28] C.K. Costello, J. Guzman, J.H. Yang, Y.M. Wang, M.C. Kung, B.C. Gates, H.H. Kung, *J. Phys. Chem. B* **2004**, *108*, 12529.

Table 1. Kinetic isotope effects for formic acid decomposition at 353 K with Pt/Al_2O_3 (d=0.21, 4 kPa) and Au/Al_2O_3 (d=0.28, 2 kPa).

	Kinetic Isotope Effect	
	Pt/Al_2O_3	Au/Al_2O_3
HCOOD	1.1	1.6
DCOOH	1.7	2.5
DCOOD	2.1	4.7

Scheme 1. Proposed elementary steps for HCOOH dehydrogenation on well-dispersed Au species.

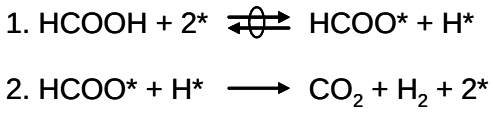

Figure 1. Arrhenius plot for HCOOH decomposition (mol h^{-1} g-at $metal^{-1}$) on Au/Al_2O_3 (2 kPa HCOOH) and Pt/Al_2O_3 (4 kPa HCOOH).

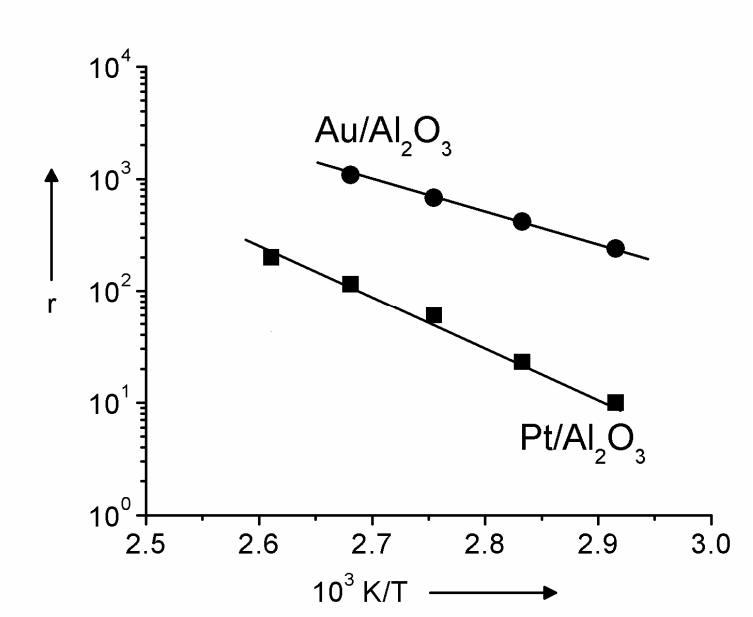

Figure 2. Turnover rates (mol s^{-1} g-at $metal_s^{-1}$) calculated from TEM-visible clusters for HCOOH decomposition on Au/Al_2O_3 (●, 2 kPa HCOOH) and Pt/Al_2O_3 (■, 4 kPa HCOOH) at 353 K.

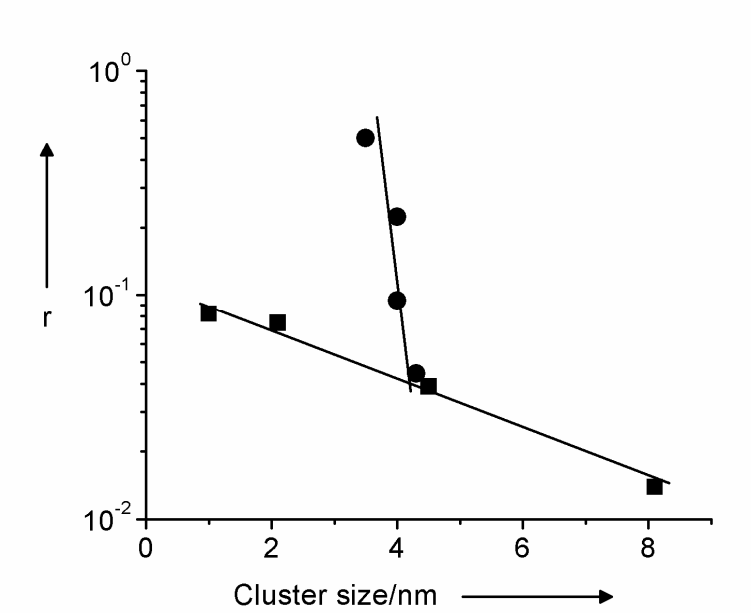

Figure 3. Influence of treatment temperature on rates (mol h^{-1} g-at Au^{-1}) for CO oxidation (●, 288 K, 5 kPa CO, 2 kPa O_2, 0.5 kPa H_2O), HCOOH decomposition (■, 353 K, 2 kPa), water-gas shift (▲, 523 K, 5 kPa CO, 2 kPa H_2O) on Au/Al_2O_3 and Au cluster size from TEM (♦).

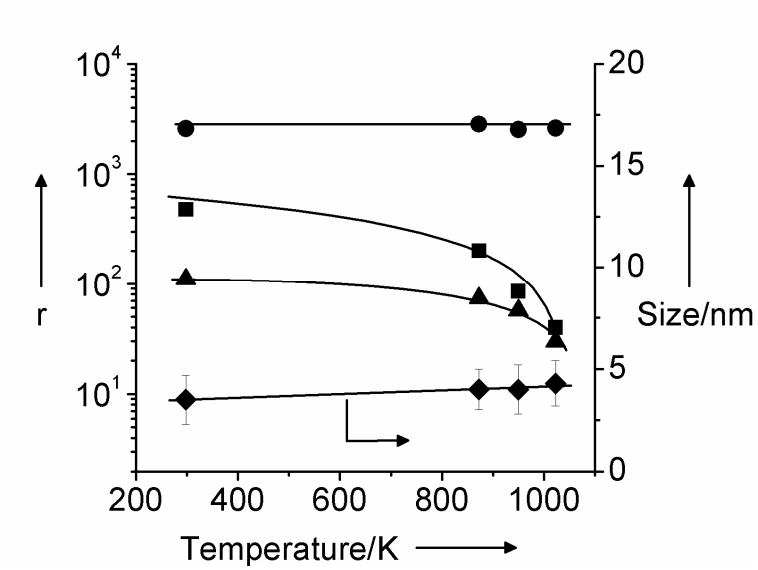

Figure 4. Effect of HCOOH partial pressure on the reaction rate (mol h^{-1} g-at $metal^{-1}$) with Au/Al_2O_3 and Pt/Al_2O_3 at 353 K.

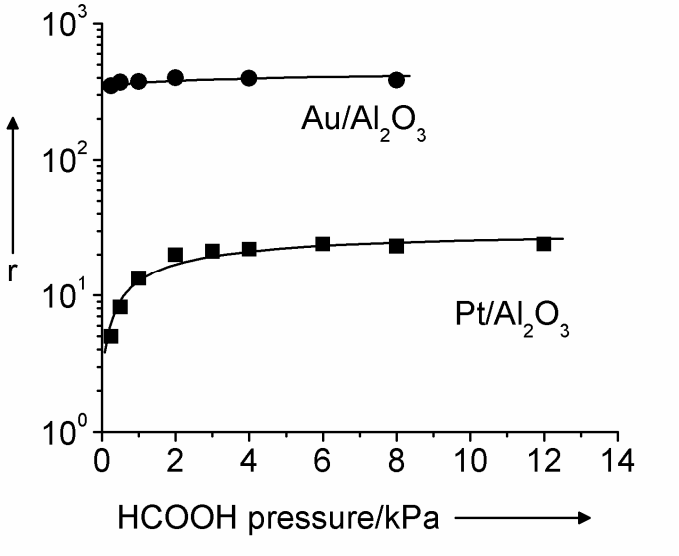

Table of Contents

HCOOH conversion to H_2/CO_2: dispersed Au species grafted onto γ-Al_2O_3 catalyze HCOOH dehydrogenation more effectively than Pt clusters, previously reported as the most active metal. Dehydrogenation occurs via H-assisted formate decomposition on Au species undetectable by microscopy. No CO is detected in H_2/CO_2 products, making them suitable for use in low-temperature fuel cells. The kinetic relevance of H_2 formation steps leads to high hydrogen chemical potentials at active sites, which may be useful in cross-hydrogenation and deoxygenation catalysis.

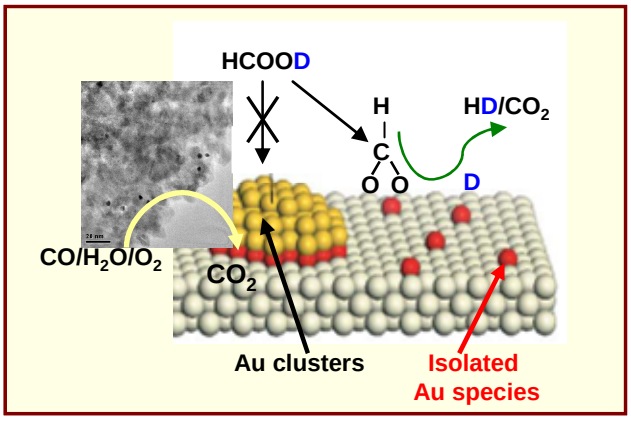

Keywords: formic acid, fuel cells, gold, heterogeneous catalysis, mechanism.

Supporting Information

Figure 1. TEM pictures and histogram of Au cluster size distribution obtained with Au/Al_2O_3 treated in O_2/He at 298 K for 2 h.

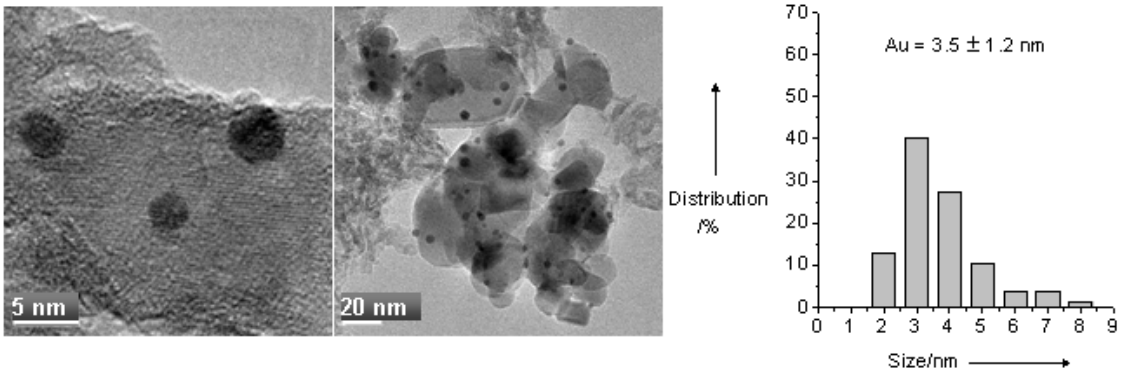

Figure 2. TEM pictures and histogram of Au cluster size distribution obtained with Au/Al_2O_3 treated in O_2/He at 873 K for 2 h.

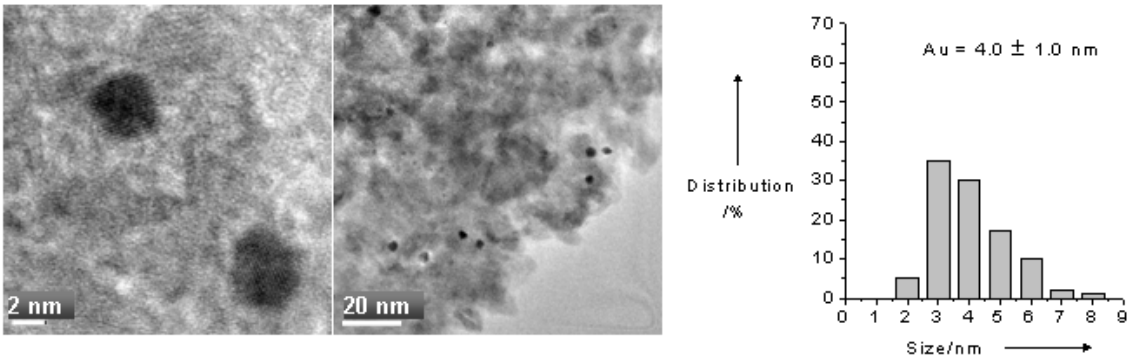

Figure 3. TEM pictures and histogram of Au cluster size distribution obtained with Au/Al_2O_3 treated in O_2/He at 950 K for 2 h.

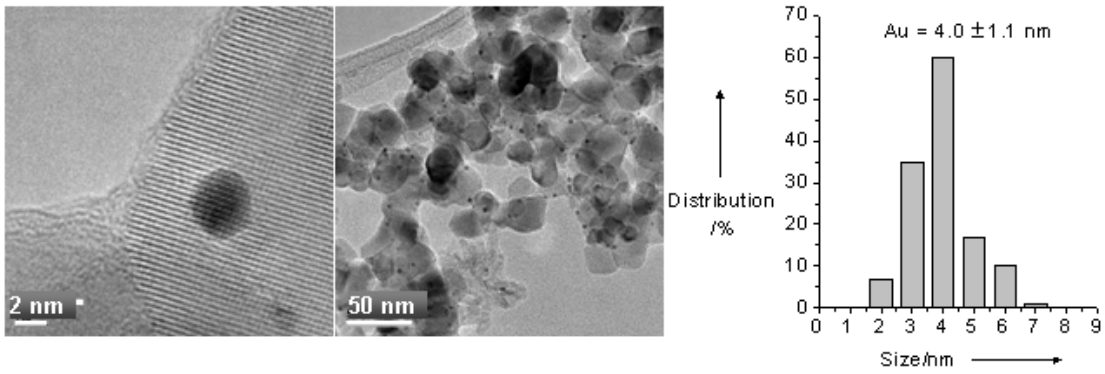

Figure 4. TEM pictures and histogram of Au cluster size distribution obtained with Au/Al_2O_3 treated in O_2/He at 1073 K for 2 h.